

Determination of the weaker phase in the pitting corrosion of non-standard low-Ni high-Mn-N duplex stainless steels

R. Merello, F. J. Botana*, J. Botella, and M. Marcos

In this paper, the use of Energy Dispersive Spectrometry (EDS) is proposed to determine the partition coefficients of the elements of a new family of duplex stainless steels that are characterized by having low contents of nickel, together with high levels of manganese and nitrogen.

From the values of the partition coefficients, the chemical compositions of the constituting phases have been determined, in order subsequently to calculate the value of the Pitting Resistance Equivalent Number (PREN) of each phase. The proposition put forward in this study is that the phase having the lower PREN determines the pitting corrosion behaviour of these types of steels.

Results obtained by means of optical and scanning electron microscopy have provided confirmation that the pitting corrosion behaviour of these new materials gets determined by the resistance of the weaker phase and consequently by the phase having the lower PREN value.

Lastly it has been proved possible to determine the existence of an exponential relationship between the alloys pitting potential (E_p) and the weaker phase PREN; this can be utilized for the low-nickel duplex stainless steels design in which the pitting corrosion resistance is controlled.

1 Introduction

The ferritic-austenitic duplex stainless steels are characterized by having a biphasic microstructure, composed of ferrite (α , with cubic structure centered on the body) and of austenite (γ , with cubic structure centered on the faces). The ratio between these two phases is usually 50% in volume, although it can vary between 30 and 70%, and more frequently between 40 and 60% [1, 2]. In chloride media, the characteristics of these materials are their resistance to intergranular corrosion, localized corrosion (pitting and crevices), and to stress corrosion, that are superior to that of austenitic steels of the AISI 300 grade. In addition, they present higher mechanical properties.

It is known that in duplex stainless steels the alloying elements are distributed unequally between the phases. The distribution is a function of the α or γ phase promoter character of these elements and of the types of heat treatment to which the materials have been subjected. In all these alloys, chromium, molybdenum and silicon are usually concentrated to a greater degree in the ferrite phase, whereas nickel, manganese and

copper are found more in the austenite. Nitrogen, in turn, is basically concentrated in the austenite phase, since its solubility is limited in the ferrite phase [3–8]. The different distribution of the elements in the phases can give rise to differences in their resistance to pitting corrosion. In this way, one of the phases will be weaker and, therefore, more susceptible to undergoing processes of pitting corrosion [5, 9].

In reference [10] a study of the pitting corrosion behaviour of a series of new duplex stainless steels of low nickel content is conducted. In the present paper, in order to check which of the phases is the determinant of the behaviour of these steels with respect to pitting corrosion, the quantitative analysis of the chemical composition of the constituting phases was determined by means of X-ray Energy Dispersive Spectrometry (EDS). The partition coefficients of the elements are determined from these data; this coefficient is calculated as the quotient between the contents of the element (% by mass) in the ferrite and austenite phases [3, 11–13].

The results obtained indicate that the partition coefficients show practically no variation in the various alloys studied. For this reason, they can be used reliably for the determination of the phases chemical compositions of all the duplex alloys.

2 Experimental

A series of 33 low in nickel duplex stainless steels were designed, with variable contents of Cr, Mo and N, holding constant the content of the rest of the elements, with the exception of the Ni (Tables 1 and 2). The content of Ni was utilized to adjust the percentage of the alloys ferrite (% α) to within the range of 40–60% following heat treatment for homogenization.

The criteria followed for the fabrication of the new duplex stainless steels is described in [14]. In addition, two standard

* F. J. Botana, M. Marcos
Departamento de Ciencia de los Materiales e Ingeniería Metalúrgica y Química, Inorgánica.
Universidad de Cádiz. Facultad de Ciencias del Mar.
Avda. República Saharaui s/n, E-11510, Puerto Real, Cádiz (Spain)

R. Merello, J. Botella
ACERINOX, S.A. Departamento Técnico.
Apdo. 83, E-11370, Los Barrios, Cádiz (Spain)

Table 1. Compositional range of the manufactured low-nickel duplex stainless steels

| % α | Si | Mn | Ni | Cu | Cr | % by mass Mo | C | S | N |
|------------|-----|----|---------|----|--------------|--------------|-------------|--------------|------------------|
| 40–60 | 0.5 | 8 | 0.5–2.7 | 1 | 18–24 | 0.3–4 | ≤ 0.03 | ≤ 0.002 | 0.09–0.34 |

Table 2. low-nickel duplex alloys contents of Cr, Mo, N and Ni and the percentage of ferrite phase

| Alloy | Cr | Mo | % by mass N | Ni | % α |
|-------|-------|------|-------------|------|------------|
| BN1 | 17.97 | 1.98 | 0.0893 | 2.44 | 49.68 |
| BN2 | 18.97 | 1.02 | 0.0998 | 1.34 | 60.66 |
| BN3 | 19.05 | 1.06 | 0.1066 | 2.42 | 43.27 |
| BN4 | 19.36 | 1.17 | 0.1132 | 2.70 | 48.41 |
| BN5 | 19.95 | 1.03 | 0.1388 | 1.05 | 60.75 |
| BN6 | 19.86 | 2.98 | 0.1747 | 1.66 | 57.66 |
| BN7 | 20.01 | 3.00 | 0.1804 | 1.64 | 61.54 |
| BN8 | 20.86 | 0.51 | 0.2123 | 0.84 | 50.23 |
| BN9 | 20.98 | 1.00 | 0.1803 | 1.04 | 62.55 |
| BN10 | 20.92 | 2.00 | 0.2305 | 1.53 | 53.16 |
| BN11 | 21.00 | 2.00 | 0.2358 | 1.55 | 52.31 |
| BN12 | 20.82 | 2.00 | 0.2487 | 0.60 | 51.70 |
| BN13 | 20.96 | 1.99 | 0.2568 | 0.55 | 51.73 |
| BN14 | 21.00 | 2.96 | 0.2558 | 1.54 | 51.73 |
| BN15 | 20.92 | 3.93 | 0.2744 | 1.34 | 53.55 |
| BN16 | 21.96 | 0.29 | 0.2209 | 2.46 | 45.50 |
| BN17 | 21.89 | 0.29 | 0.2355 | 0.55 | 53.96 |
| BN18 | 21.92 | 0.99 | 0.2213 | 1.56 | 51.67 |
| BN19 | 21.89 | 0.98 | 0.2218 | 1.65 | 55.78 |
| BN20 | 21.98 | 1.90 | 0.2309 | 1.27 | 57.39 |
| BN21 | 21.95 | 3.01 | 0.2360 | 1.85 | 55.68 |
| BN22 | 22.10 | 2.98 | 0.2561 | 1.84 | 60.07 |
| BN23 | 22.02 | 3.04 | 0.2586 | 1.76 | 54.15 |
| BN24 | 22.46 | 2.61 | 0.2613 | 1.65 | 54.96 |
| BN25 | 21.97 | 3.00 | 0.3411 | 1.06 | 50.28 |
| BN26 | 21.89 | 3.97 | 0.2468 | 2.05 | 56.42 |
| BN27 | 21.77 | 4.03 | 0.2863 | 2.03 | 54.30 |
| BN28 | 22.90 | 1.03 | 0.2172 | 1.73 | 61.22 |
| BN29 | 22.89 | 1.00 | 0.2434 | 1.75 | 56.42 |
| BN30 | 22.89 | 2.00 | 0.2406 | 2.18 | 59.65 |
| BN31 | 22.86 | 2.99 | 0.3066 | 1.54 | 53.47 |
| BN32 | 22.99 | 3.01 | 0.3191 | 1.55 | 53.53 |
| BN33 | 23.96 | 3.04 | 0.2896 | 2.59 | 57.74 |

duplex stainless steels were also manufactured for reference purposes, 2304 (DC1) and 2205 (DC2), Table 3.

The alloys were fabricated in the form of 50 grams ingots in a LIFUMAT MET 3.3 VAC centrifugal casting induction oven. All the alloys were heat-treated for homogenization at 1100 °C for 30 minutes.

2.1 Microanalysis using EDS

To perform the EDS study, a Field Effect Scanning Electron Microscope (FESEM) equipped with a microanalysis system was used.

From the alloys prepared, those designated BN2, BN3, BN15, BN16, BN29, BN31, DC1 and DC2 were selected for the microanalysis study and the determination of partition coefficients. Their chemical compositions are given in Table 3. A test piece with a cross section of approximate dimensions of 6 mm \times 33 mm was cut from the ingots of each of these materials and used for the microanalysis.

The cross section of each test piece was polished to mirror finish, and a total of 200 EDS spectra were acquired; these were distributed along a straight line at a distance of 50 μ m from the upper edge, as shown in Fig. 1. The positions of the first and last points of this line were set manually and the rest of the positions were established automatically, such that the approximate distance between two adjacent points was 0.12 mm. The spectra at each of the points were acquired in the conditions indicated in Table 4. To correct the small instabilities or deflections of the electron source, the spectrum of a Co standard was obtained at intervals of 1 hour.

Once the spectra had been acquired, they were classified as corresponding either to ferrite or austenite following a statistical method of treatment of the spectra described in [3]. To perform this classification it was necessary to obtain spectra considered as standards. These spectra were recorded using sufficiently large grains of ferrite and austenite. The conditions under which the standards were recorded were the same as those utilised in the study of the working samples. The lines utilised to compare the standard spectra with those of the samples were the $K\alpha$ corresponding to Mo, Si, N and Cu (Fig. 2).

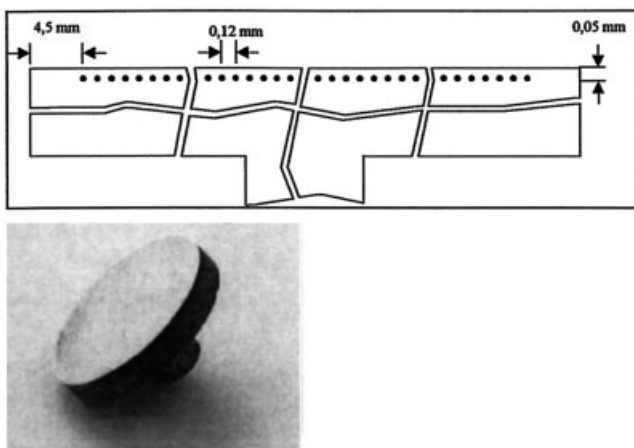
The chemical composition of each phase was calculated by means of the ZAF method which considered the effect of different factors (atomic number, z , matrix absorption, A and fluorescence, F) [15, 16]. In the procedure devised in [3], it is proposed to refine the composition of each phase by eliminating those spectra that might be derived from mixtures of phases. In this way, it is considered that the chemical composition of the austenite phase of each material will be the result of averaging the composition of all the points whose spectra present a high degree of fit to that of the austenite standard. Similarly, the composition of the ferrite phase will be the average of the points with a chemical composition corresponding to that of the ferrite grains.

2.2 Electrochemical measurements

In accordance with the conducted study [10], the evaluation of the resistance to pitting corrosion was performed by the determination of the potential corresponding to a pitting current density of 100 μ A/cm², E_p , (mV vs SCE) in a chloride medium (50 g/l NaCl, 50 °C). Potentiodynamic trials were carried out with a scanning rate of 0.17 mV/s [17–19], utiliz-

Table 3. Chemical compositions of the microanalysed low-nickel and standard duplex stainless steels

| Ident. | % by mass | | | | | | | | |
|--------|-----------|------|--------|------|------|------|------|-------|--------|
| | Cr | Mo | N | Si | Mn | Ni | Cu | C | S |
| BN2 | 18.97 | 1.02 | 0.0998 | 0.57 | 8.18 | 1.34 | 1.06 | 0.024 | 0.0015 |
| BN3 | 19.05 | 1.06 | 0.1066 | 0.49 | 8.58 | 2.42 | 1.08 | 0.023 | 0.0016 |
| BN15 | 20.92 | 3.93 | 0.2744 | 0.50 | 8.23 | 1.34 | 1.07 | 0.026 | 0.0015 |
| BN16 | 21.96 | 0.29 | 0.2209 | 0.58 | 8.17 | 2.46 | 1.02 | 0.023 | 0.0015 |
| BN29 | 22.89 | 1.00 | 0.2434 | 0.54 | 8.08 | 1.75 | 1.04 | 0.025 | 0.0017 |
| BN31 | 22.86 | 2.99 | 0.3066 | 0.52 | 8.28 | 1.54 | 1.06 | 0.028 | 0.0015 |
| DC1 | 22.55 | 0.29 | 0.0815 | 0.52 | 0.97 | 4.03 | 0.31 | 0.023 | 0.0017 |
| DC2 | 21.06 | 2.46 | 0.1011 | 0.68 | 1.66 | 5.52 | 0.30 | 0.025 | 0.0010 |

**Fig. 1.** Ingot of 50 grams and diagram of the cross section point positions at which the microanalysis were performed

ing for this a potentiostat/galvanostat controlled by a PC running the "Model 352 SoftCorr III" software.

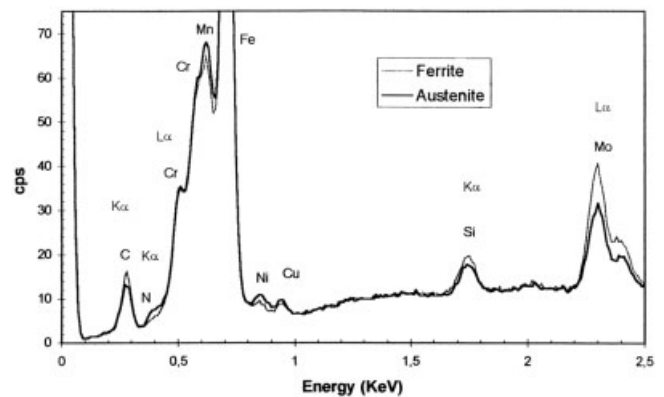
3 Results

Once the EDS spectra had been obtained for each of the materials, they were classified as belonging either to the ferrite or the austenite phase. Then the average chemical composition of each phase was determined. The results were submitted to the refining procedure proposed in [3].

From these data, the values of the partition coefficients of the elements and their mean value were calculated for each alloy (Table 5). As it can be observed in this table, for the annealing temperature of 1100 °C, the values obtained for the partition coefficients in the low-nickel duplex stainless steels do not differ from those corresponding to the standard duplex

Table 4. Acquisition conditions of the X-ray spectra

| | |
|------------------|----------|
| Energy range | 0–10 keV |
| Acquisition time | 300 s |
| Magnifications | × 10 000 |
| Potential | 15 keV |
| Working distance | 10 mm |

**Fig. 2.** Comparison of austenite and ferrite standard spectra

stainless steels. For the duplex alloys in general, the partition coefficients have similar values and appear to depend neither on the chemical composition nor on the content of phases present. These results demonstrate, therefore, that the partition coefficients show practically no variation in either the new duplex alloys or in the standard duplex alloys.

From the calculated Cr and Mo partition coefficients, the global chemical composition of the manufactured duplex alloys and the percentages of phases present in each alloy, it was possible to calculate the contents of these elements in the ferrite and austenite phases. Given that the technique utilised does not allow the nitrogen to be quantified with precision, it was considered that it has a limit of solubility of 0.05% in the ferrite phase; this value has been utilized by various authors [3–8].

The PREN value in each of the phases has been calculated. To perform this calculation the following equation was applied:

$$\text{PREN} = \% \text{Cr} + 3.3\% \text{Mo} + 16\% \text{N} \quad (1)$$

This equation is proposed in references [5, 7, 8, 11] for different duplex stainless steels. Table 6 includes the calculated PREN values for the low-nickel duplex alloys and Table 7 the values corresponding to the standard duplex alloys. These tables also include the pitting potential mean value of each alloy, determined by means of potentiodynamic trials in a sodium chloride medium (50 g/l, 50 °C) [10].

In general, for low-nickel duplex alloys, the ferrite phase PREN values are lower than those of the austenite phase.

Table 5. Partition coefficients of elements for the microanalysed alloys and mean values

| Alloy | % α | Si | Cr | Mn | Fe | Ni | Cu | Mo |
|--------------|------------|-------|-------|-------|-------|-------|-------|-------|
| BN3 | 43.27 | 1.11 | 1.19 | 0.89 | 0.98 | 0.66 | 0.74 | 1.57 |
| BN16 | 45.50 | 1.16 | 1.15 | 0.90 | 0.98 | 0.69 | 0.77 | * |
| BN31 | 53.47 | 1.24 | 1.06 | 0.88 | 0.99 | 0.70 | 0.77 | 1.52 |
| BN15 | 53.55 | 1.21 | 1.06 | 0.87 | 0.99 | 0.70 | 0.76 | 1.52 |
| BN29 | 56.42 | 1.18 | 1.10 | 0.87 | 0.99 | 0.68 | 0.73 | 1.50 |
| BN2 | 60.66 | 1.11 | 1.17 | 0.88 | 0.98 | 0.67 | 0.75 | 1.58 |
| DC3 | 47.87 | 1.14 | 1.16 | 0.87 | 0.97 | 0.64 | * | 1.58 |
| DC1 | 62.34 | 1.13 | 1.17 | 0.89 | 0.98 | 0.65 | * | * |
| Mean value | | 1.16 | 1.13 | 0.88 | 0.98 | 0.67 | 0.75 | 1.54 |
| Std Dev. (s) | | 0.048 | 0.054 | 0.011 | 0.008 | 0.022 | 0.018 | 0.035 |
| Max. | | 1.24 | 1.19 | 0.90 | 0.99 | 0.70 | 0.77 | 1.58 |
| Min. | | 1.11 | 1.06 | 0.87 | 0.97 | 0.64 | 0.73 | 1.50 |

* In these cases it was not possible to determine the partition coefficients since the error associated to the estimation of the average content of the element was greater than its level in the alloy

In contrast, in the alloys BN1, BN2, BN3, BN4, BN5, BN6, BN7 and BN26, the PREN of the austenite phase is lower than that of the ferrite phase. These alloys are characterised by having a nitrogen content of less than 0.18% (except for alloy BN26). Also, in these alloys the Cr and Mo contents of the

ferrite phase are higher than those of the austenite phase. This means that, for these alloys, the PREN values for the ferrite are higher than for the austenite. In the particular case of the duplex BN26, although the level of nitrogen is relatively high (0.247%), its contents of Cr and Mo are also high and make that the ferrite becomes more resistant.

Table 6. PREN values for the ferrite (α) and austenite (γ) phases of the low-nickel duplex alloys and pitting potential mean value (Ep)

| Alloy | PREN α | PREN γ | Ep (mV vs SCE) |
|-------|---------------|---------------|----------------|
| BN1 | 27.83 | 24.06 | 112 |
| BN2 | 24.58 | 22.93 | 111 |
| BN3 | 25.55 | 23.25 | 84 |
| BN4 | 26.11 | 24.03 | 128 |
| BN5 | 25.66 | 25.47 | 124 |
| BN6 | 33.27 | 31.46 | 372 |
| BN7 | 33.20 | 32.15 | 320 |
| BN8 | 24.97 | 26.92 | 119 |
| BN9 | 26.51 | 28.21 | 143 |
| BN10 | 30.84 | 31.65 | 299 |
| BN11 | 30.96 | 31.82 | 291 |
| BN12 | 30.79 | 32.02 | 275 |
| BN13 | 30.92 | 32.41 | 272 |
| BN14 | 34.81 | 34.90 | 445 |
| BN15 | 38.42 | 38.10 | 500 |
| BN16 | 25.43 | 27.32 | 118 |
| BN17 | 25.06 | 28.44 | 99 |
| BN18 | 27.96 | 29.56 | 148 |
| BN19 | 27.69 | 29.90 | 151 |
| BN20 | 31.31 | 32.82 | 335 |
| BN21 | 35.70 | 35.58 | 426 |
| BN22 | 35.41 | 36.94 | 439 |
| BN23 | 36.01 | 36.37 | 533 |
| BN24 | 34.73 | 35.88 | 418 |
| BN25 | 36.13 | 38.55 | 496 |
| BN26 | 39.35 | 38.42 | 971 |
| BN27 | 39.66 | 39.65 | 979 |
| BN28 | 28.71 | 31.45 | 170 |
| BN29 | 32.50 | 34.57 | 393 |
| BN30 | 28.82 | 31.76 | 233 |
| BN31 | 36.78 | 38.63 | 552 |
| BN32 | 36.98 | 39.23 | 638 |
| BN33 | 37.77 | 39.76 | 881 |

In the low-nickel duplex alloys BN14, BN15, BN21 and BN27, the chemical composition is balanced so that similar PREN values are obtained of the two phases.

Regarding the standard duplex alloys, the data (Table 7) indicate that in all cases the austenite phase presents PREN values lower than the ferrite phase one.

The nitrogen content plays a very important role in the definition of the weaker phase and, therefore, determines the corrosion pitting behaviour of duplex stainless steels. In general, in those duplex alloys with low nitrogen content, the austenite phase has a PREN value lower than that of the ferrite phase, since the ferrite is richer in Cr and Mo [12, 20]. This occurs in the low-nickel duplex alloys BN1, BN2, BN3, BN4, BN5, BN6 and BN7, as well as in the standard duplex alloys DC1 and DC2, whose nitrogen content in both cases is less than 0.18%.

However, when the nitrogen content of the low-nickel duplex alloys increases, nitrogen is concentrated preferentially in the austenite phase, because its solubility in the ferrite phase is limited [3, 5–8]. Hence the PREN value of the austenite may equal or even exceed that of the ferrite phase.

When it comes to designing a duplex steel, it is important to take this fact into account, since if the two phases do not have approximately the same PREN value, the alloy's resistance to pitting corrosion will be given by the PREN of the weaker

Table 7. PREN values for the ferrite (α) and austenite (γ) phases of the standard duplex alloys and pitting potential (Ep)

| Alloy | PREN α | PREN γ | Ep (mV vs SCE) |
|-------|---------------|---------------|----------------|
| DC1 | 25.49 | 23.72 | 282 |
| DC2 | 33.49 | 28.73 | 594 |
| DC3 | 35.97 | 31.44 | * |

* This alloy does not suffer pitting corrosion in this medium

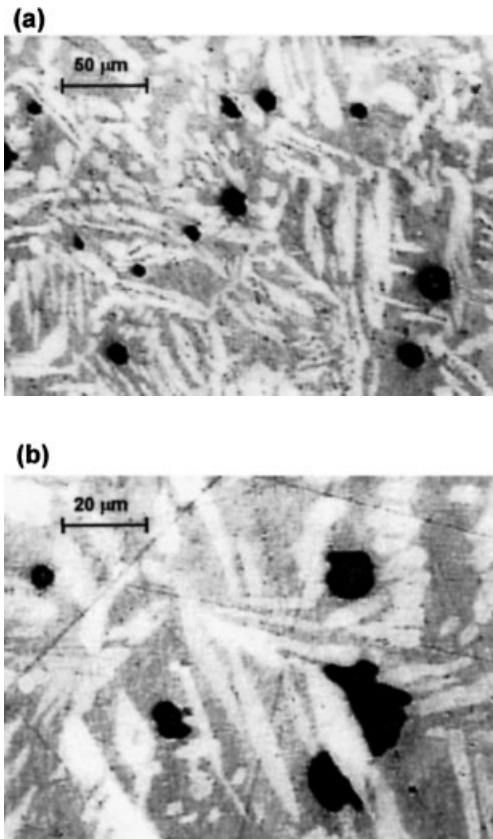


Fig. 3. Images of the duplex alloy BN30 acquired using an optical microscope. Depiction of the surfaces potentiodynamically tested in a solution of 50 g/l NaCl and at a temperature of 50 °C

phase and, therefore, will be less than that estimated by the PREN value calculated from the global chemical composition of the stainless steel.

With the aim of confirming if the phase with the lower PREN is the one that conditions the initiation and development of the pits in the low-nickel duplex alloys, experiments were performed that consisted of revealing the structure of the samples after having submitted them to anodic polarization trials until the pitting potential was reached. The reagent utilized to reveal the structure was an acidified potassium bisulfite solution [21].

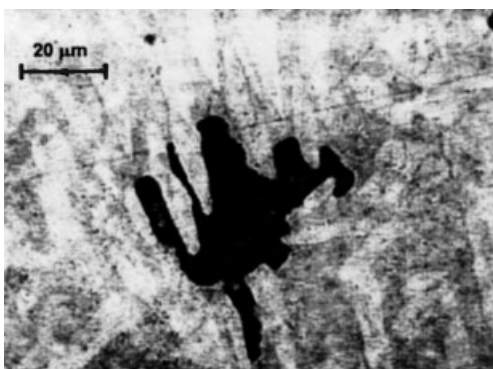


Fig. 4. Image of the duplex alloy BN22 acquired using an optical microscope. Depiction of the surfaces potentiodynamically assayed in a solution of 50 g/l NaCl and at a temperature of 50 °C

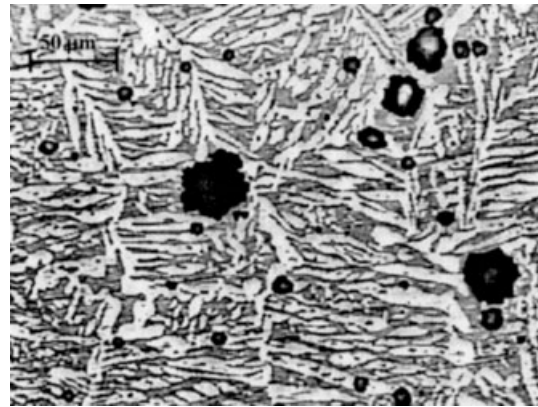


Fig. 5. Image of the duplex alloy BN4 acquired using an optical microscope. Depiction of the surfaces potentiodynamically assayed in a solution of 50 g/l NaCl and at a temperature of 50 °C

The samples thus obtained were observed using an optical microscope. In Fig. 3 the images obtained on revealing the structure of the alloy BN30 are presented. The high nitrogen content of this alloy makes the austenite PREN being higher than that of the ferrite phase. It can be observed that the pits found in the tested surface appear on the ferrite phase (dark color). There has been a selective dissolution of this phase and the pits are developed without affecting the grains of austenite that appear intact in these images.

This same type of behaviour has been observed in the alloys BN22 and BN10, in which the PREN ferrite values are lower than those of the austenite phases. In the image shown in Fig. 4 it can be seen how the pit growth is produced by dissolution of the ferrite, but the grains of austenite are not attacked.

Fig. 5 shows the image obtained on revealing the structure of the alloy BN4 after the anodic polarization trial. This alloy has a low nitrogen content and its austenite phase presents a PREN lower than that of the ferrite. In this case, it can be seen that pits of smaller size have been produced in the grains of austenite, from which it can be deduced that the attack initiated on this phase. However, as the pits grew, they did so affecting both phases similarly, unlike the process observed on the sample previously discussed.

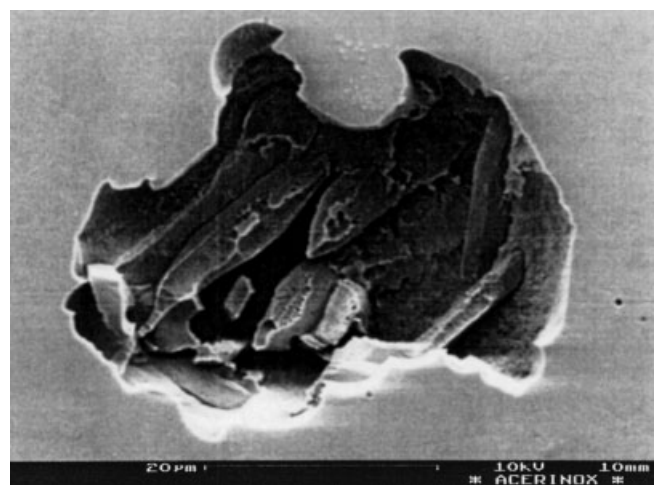


Fig. 6. Image by secondary electrons from a pit of the duplex alloy BN30

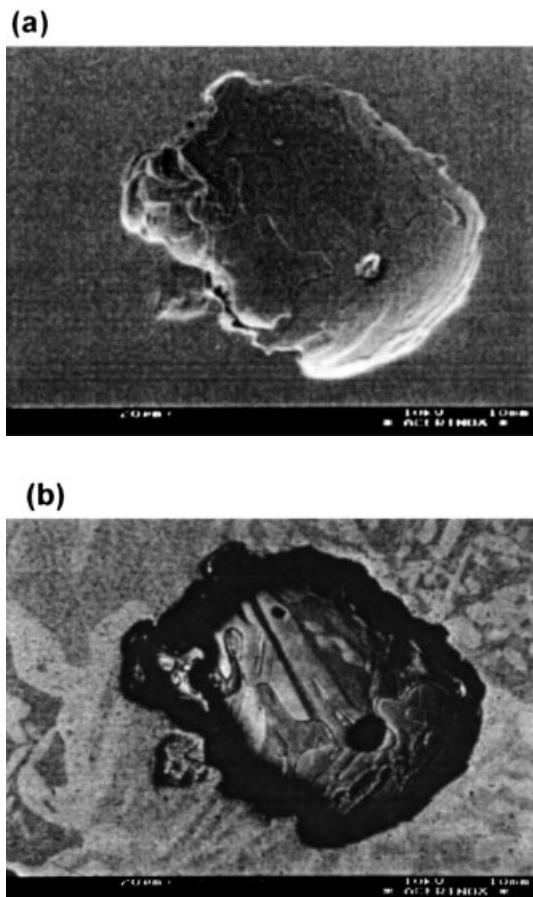


Fig. 7. Images by secondary electrons (a) and retrodispersed electrons (b) from a pit of the material BN1

Observations with the electron microscope were made of other low-nickel duplex alloys, after having submitted them to anodic polarization trials in a solution of 50 g/l of sodium chloride at 50 °C, to provoke the formation of pits.

The alloy BN30 surface thus treated was observed in the electron microscope; the PREN of this alloy's ferrite phase is lower than that of the austenite. The secondary electron image obtained of one of the pits that developed in the potenti-

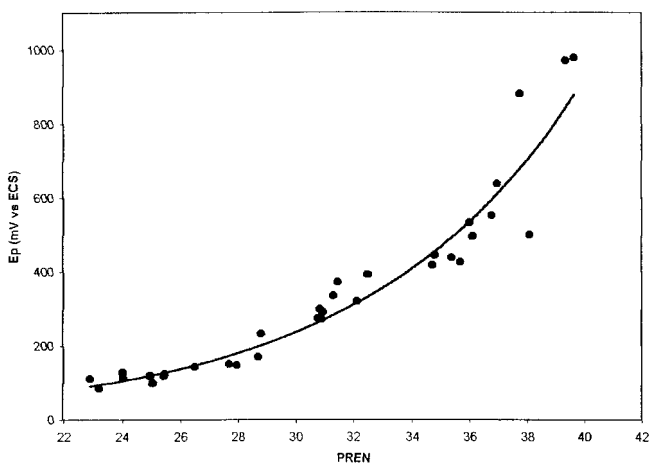


Fig. 8. Exponential fit obtained between the pitting potentials (E_p) and the weakest phases PREN values

Table 8. Results of the regression analysis between the pitting potentials (E_p) and the PREN values of the weakest phases of the low-nickel duplex alloys

| | Parameter | Estimate | Error | “Student” t | Probability |
|------|-----------|----------|-----------|-------------|-------------|
| PREN | Intercept | 1.40102 | 0.161372 | 8.68193 | 0.0000 |
| | Slope | 0.135672 | 0.0051172 | 26.5128 | 0.0000 |
| | r^2 | | | 95.7761 | |
| | S_y | | | 0.148338 | |

dynamic trial is shown in Fig. 6. The crystals that remained undissolved inside the pit were analysed by DES; it was confirmed that they were grains of austenite. This alloy has a homogeneous microstructure consisting of 59.65% of ferrite and 40.35% of austenite phases. The fact of finding only crystals of austenite in the interior of the pit seems to indicate that a selective dissolution of the ferrite phase has taken place.

Further, Fig. 7 shows the electron microscope images of the alloy BN1 tested surface. This alloy austenite PREN is lower than that of the ferrite phase. The secondary electron image (Fig. 7a) shows one of the pits found. Retro-dispersed electron image were obtained of this same pit (b), and it was found that grains of both ferrite (dark color) and austenite (light color) could be distinguished in the interior of the pit. This finding would imply that the selective solution of one the phases had not taken place.

These results confirm that the initiation of pitting corrosion in these new materials is determined by the resistance of the weaker phase and consequently by the resistance of the phase with the lower PREN value.

With the aim of establishing what kind of relationship exists between the alloy pitting potential and the PREN value of the weaker phase, a regression was performed between this latter parameter and the pitting potential mean values of the low-nickel duplex steels, Table 6. It can be seen in Fig. 8 that it exists an exponential-type mathematical relationship between the two variables. Table 8 gives the results of this regression analysis.

The resulting exponential equation obtained from the regression of the pitting potentials (E_p) and the PREN values of the weaker phase, is the following:

$$E_p = \exp (1.40 + 0.14 \text{ PREN}) \quad (2)$$

Making use of this equation, it is possible to determine the pitting potentials of low-nickel duplex alloys from the PREN values of the weaker phase and to design this type of alloys with pitting corrosion resistance equivalent or superior to that of standard duplex stainless steels.

4 Conclusions

The obtained results indicate that EDS quantitative analysis enables the determination of the ferrite and austenite average chemical composition in the low-nickel duplex stainless steels. The followed procedure is based on the determination of the partition coefficients from the EDS spectra. The obtained values for this parameter show practically no variation between the different duplex stainless steels studied. Thus, by making use of these coefficients, the global chemical composition and the percentage of each phase, it is possible to determine the phases chemical compositions of any duplex alloy.

Having established these compositions, the Pitting Resistance Equivalent Number (PREN) of each phase has been determined. Samples that underwent pitting corrosion were studied by microscopy. The results indicated that the initiation of pits on these materials took place in the weaker phase. Thus, when the ferrite was the weaker phase, the pit initiated on this phase and its development took place through this phase selective dissolution. When the austenite was the weaker phase, the initiation of the pit took place in this phase, although the pit grew by the solution of both phases.

Lastly, it has been found that an exponential relationship exists between the pitting potential of each alloy and the weaker phase chemical composition, expressed through its PREN. Application of this equation provides an estimate of the resistance to pitting corrosion of the new alloys, and allows for the design of new low-nickel duplex alloys with a resistance to pitting corrosion equivalent or superior to that of the standard duplex steels.

5 References

- [1] S. Gutiérrez de Sáinz-Solabarriá, I. Gutiérrez Urrutia, J. M. San Juan Nuñez, *Química e Industria* (Quibal) **1999**, 90.
- [2] G. Di Caprio, *Ed. Grupinox*, Barcelona **1999**, 17.
- [3] I. Moreno, *Ph. D. Doctoral Thesis*, University of Sevilla, **2001**.
- [4] A. Van Bennekom, *Stainless Steel World*, Dec. **1998**, 54.
- [5] L. F. Garfias-Mesias, J. M. Sykes, C. D. S. Tuck, *Corrosion Science*, **1996**, 38, 1319.
- [6] C. D. S. Tuck, J. M. Sykes, L. F. Garfias-Mesias, *TWI paper 15*, Glasgow, **1994**.
- [7] S. Gutiérrez de Sáinz-Solabarriá, J. M. San Juan Nuñez, *Deformación metálica* **1996**, 226, 77.
- [8] C. D. S. Tuck, L. F. Garfias-Mesias, J. M. Sykes, *DSS Proceedings* **1997**, 683.
- [9] H. Vannevik, J. O. Nilsson, J. Frodigh, P. Kangas, *ISIJ International*, **1996**, 36, 807.
- [10] R. Merello, J. Botana, J. Botella, M. Marcos, V. Matres, *Submitted to Corrosion Science*.
- [11] J. Charles, *DSS Proceedings*, Beaune, France **1991**, 1, 3.
- [12] J. Charles, *Welding in the World* **1995**, 36, 43.
- [13] J. G. Potgieter, M. B. Cortie, *Materials Characterization* **1991**, 26, 155.
- [14] *Patente Española no 200002019*. Acero Inoxidable Dúplex Austeno-Ferrítico con Bajo Contenido en Níquel. Agosto **2000**.
- [15] J. W. Colby, *Adv. X-Ray Anal.* **1968**, 11, 287.
- [16] Ch. Poehn, J. Wernisch, W. Henke, *X-Ray Spectrometry* **1985**, 14, 120.
- [17] *ASTM G 61-86*.
- [18] *ASTM G 5-94*.
- [19] R. Bandy, D. Van Rooyen, *Corrosion* **1983**, 39, 227.
- [20] S. Bernhardsson, *DSS Proceedings* Beaune **1991**, 1, 185.
- [21] E. Weck, E. Leistner, *Metallographische Anleitung zum Farbätzen nach dem Tauchverfahren*, part III DSV, 77/III, **1986**.

(Received: February 14, 2003)

W 3694